Sensorless Control on a Dual-Fed Flux Modulated Electric Motor

Xiang Luo, L. Zhu, Xu Cai, Weinong Fu and Xinye Wu
(Invited)

***Abstract*—This paper proposes the operation principle and a new flux estimation method for sensorless control strategy for the dual-fed flux modulated electric motor (DFFM). The DFFM is designed based on the flux modulation theory, it includes two stator windings and one rotor which simplify the mechanical structure. The rotor has only modulation iron and no permanent magnets on it, so there is no cogging torque problem in this motor. With adjustment of the outer and inner stator flux rotating frequency and amplitude, different rotation speed and torque of the sandwiched rotor can be gained for the DFFM. Furthermore, an improved flux estimation based sensorless control strategy is performed on the proposed machine to fit the two winding set control situation. The startup and performance of the proposed control strategy is verified by the simulation and experiments.**

***Index Terms*—Dual-fed flux modulated electric motor, flux estimation, flux modulation, sensorless control.**

I. Introduction

A new kind motor which is based on the effect of flux modulation has been a research hotspot in recent years as its possibility of low-speed and high-torque, as for its possibility of low-speed and high torque[1]-[14]. Generally, the Vernier motors[11], magnetic-geared permanent-magnet (PM) brushless motor[3, 9, 12], and the doubly-fed dual-rotor flux-modulation PM motors[8, 14], double-stator flux-modulation PM motor [5]and etc. are all belong to this type of motor[1, 2, 7]. Commonly, with the special motor structure to modulate the magnetic field existing in the motor, the harmonic components of the magnetic field become to play the major role in the motor, thus the rotational speed and output torque of the motor can be scaled [1, 2, 7].

The theory of the flux modulation motor is derived from the study of magnetic gears. The magnetic gear is a three-layer structure, that is, a layer of flux-modulation iron segments is sandwiched between two layers of PMs, which can replace the mechanical gear to complete the torque transmission. Based on the magnetic gear, [3] and [12] use a stator winding to replace one layer of PMs and the magnetic-geared PM brushless motor is obtained which satisfies the principle of the magnetic gear. Therefore, if the other layer of PMs are also replaced with the stator winding, the dual-fed flux-modulated electric motor (DFFM) is presented in this paper.

There is no PM inside the DFFM motor, so there is no cogging torque problem. Furthermore, as only one rotor in DFFM, the mechanical can be simplified. The two sets of stators can be each other armature and excitation windings, and the energy distribution is flexible. As for the proposed DFFM motor, the outer and inner stator flux rotating frequency and amplitude can be flexibly adjusted for different rotation speed and torque of the sandwiched rotor.

Furthermore, the position sensorless control based on field oriented control (FOC) of the proposed DFFM motor is also studied in this paper. There are many kinds of sensorless control methods based on FOC theory. In this paper, the flux estimation based FOC sensorless control method is adopted. The flux estimation algorithm has been applied to direct field-oriented sensorless control for induction motor. This type of estimation method has been proved that have advantages of robustness, steady and wide operation range [15]-[17]. Aiming at DFFM, this paper proposes an improved flux estimation observer method with consideration of the changes of phase and amplitude of the excitation current during operation. Simulation results and experimental analysis are also performed in this paper to verify the feasibility and accuracy of the proposed estimation algorithm in DFFM sensorless control.

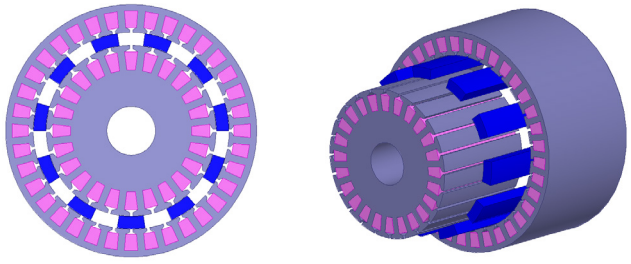

(a) (b)

Fig. 1. Configuration of the proposed DFFM motor. (a) Sectional View. (b) Three-dimensional view

II. Motor Description

The proposed DFFM motor is shown in Fig. 1. It can be noticed that there are two air gaps between the two stators

Manuscript was submitted for review on 30, January, 2019.

Xiang Luo, L. Zhu and Cai Xu are now with Key Laboratory of Control of Power Transmission and Conversion (SJTU), Ministry of Education, Shanghai, China (e-mail: maskluo@sjtu.edu.cn; L. Zhu@sjtu.edu.cn; xucai@sjtu.edu.cn).

Weinong Fu X. are with Electrical Engineering Department, Hong Kong Polytechnic University, Kowloon, Hong Kong (e-mail: eewnfu@polyu.edu.hk).

Xinye Wu are with Management Department, State Grid Shanghai Municipal Electric Power Company, Shanghai, China (e-mail: 15558171@qq.com).

Digital Object Identifier 10.30941/CESTEMS.2019.00009

(named as inner stator and outer stator) and the rotor. The outer stator core has slots of number z_1, and three phase windings with pole pair number p_1 are wound in it. On the other hand, the inner stator core has slots of number z_2, in which three phase windings with pole pair number p_2 are wound. The rotor is sandwiched between the two stators, with number N_r iron ferromagnetic segments. Its operating principle is similar with the Vernier machine in, which is based on the rule called the "magnetic gear effect". In the proposed DFFM motor, the iron segments on the rotor are designed to modulate the magnetic flux generated by the two stator windings. Thus, the magnetic flux generated by the inner stator windings is modulated by the iron segments on the rotor, and then interacts with the outer stator winding flux at the outer air gap. Meanwhile, at the inner air gap, the modulated outer stator winding flux interacts with the inner stator winding flux.

Therefore, the proposed working principle is similar with the magnetic gears, the PMs of the magnetic gear are replaced with the stator windings. To maximum the fundamental harmonic field and produce steady torque, the motor can satisfy:

$$N_r = p_1 + p_2 \tag{1}$$

As for the prototype motor in the paper, the outer stator winding pole pair number p_1 is chosen to be 6 and the inner stator winding pole pair number p_2 is chosen to be 5, thus the modulation iron segments number N_r is 11.

Similar to the magnetic gear, the frequency relationship of the rotor and the flux density space harmonics can be given by:

$$f_1 + f_2 - f_N = 0 \tag{2}$$

in which f_1 and f_2 are the outer and inner stator flux rotating frequency and f_N is the rotor rotating frequency. Thus the motor velocity n_r can be derived:

$$n_r = \frac{(f_1 + f_2) * 60}{N_r} \tag{3}$$

Therefore, with the adjustment of f_1 and f_2, the motor velocity n_r can be controlled flexibly.

The parameters of the proposed DFFM motor are listed in Table I. Based on the Finite-Element Method (FEM), the flux density in the two air gaps, the FFT analysis and no-load Back-EMF of the two windings are analyzed for the DFFM motor, as shown in Fig. 2.

In the Fig.2 (a) to (e), the 15A DC current was supplied to the inner windings to generate directional magnetic field when the motor velocity is 900rpm, the two air gap flux densities and the no-load back-EMF of the other winding were analyzed with FEM. The FFT results in (b) and (d) indicates that with the modulation of the iron ferromagnetic segments, the 5 pole-pair magnetic flux in the inner air gap is modulated to a 6 pole-pair magnetic flux in the outer air gap whose pole pair number is just the same as the pole pair number of the outer stator. Therefore, the modulated magnetic flux interacts with the outer winding, and the three phase back-EMF in the outer winding can be measured. The no-load back-EMFs of the three phases are sinusoidal, as shown in Fig.2 (e). It indicates that the no-load DC current generated flux linkages of the three phases are sinusoidal and the DFFM motor is more suitable for sinusoidal current drive.

TABLE I
PARAMETER OF THE PROPOSED DFFM

Parameter	Value
Rated Voltage (V)	220
Rated Torque (Nm)	4
Rated Speed (rpm)	924
Outer Diameter of the outer stator (mm)	182.5
Inner Diameter of the outer stator (mm)	121
Turns per phase in outer winding	15
Outer stator slot number	36
Outer stator pole pair number	6
Air gap between outer stator and rotor (mm)	1
Outer Diameter of the inner stator (mm)	106
Inner Diameter of the inner stator (mm)	30
Turns per phase in inner winding	15
Inner stator slot number	24
Inner stator pole pair number	5
Air gap between inner stator and rotor (mm)	1
Axial length (mm)	160

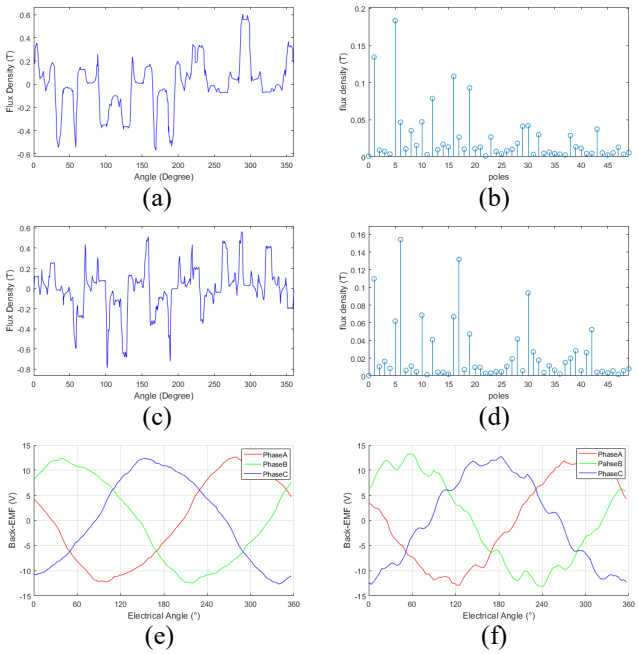

Fig. 2. FEM results of the DFFM when 15A DC current is supplied to one winding. (a) Flux density in the inner air gap when 15A DC current in inner windings; (b) FFT result of (a); (c) Flux density in the outer air gap in the same condition of (a); (d) FFT result of (c); (e) back-EMF of outer windings in the same condition of (a); (f) back-EMF of inner windings when 15A DC current in outer windings, which is opposite to (a).

When 15A DC current is supplied to the outer rotor, the back-EMF of the inner windings can be measured, as shown in Fig.2 (f). The results shown in Fig. 2 (e) and (f) indicates that the modulation function of the iron ferromagnetic segments are bidirectional, the flux linkage in the inner and outer air gap can be modulated to the other side. Either winding can be defined as field winding. The DC or sinusoidal AC current is supplied to the field winding to generate magnetic field, and the modulated magnetic field interacts with the other winding to drive the motor.

III. CONTROL SCHEME OF THE DFFM MOTOR

In this paper, the inner winding is defined as the field winding, current is supplied into this winding to generate the main magnetic field, which is modulated by the iron ferromagnetic segments and interacts with the outer winding in the outer air gap. The control scheme of the DFFM can be derived according to this setup.

A. Control scheme of the DFFM motor

The flux linkage in the outer air gap is generated by the inner winding, and modulated by the iron segments in the rotor. $\bar{\lambda}$ is defined as modulation ratio, the superscript sign '$\bar{}$' indicates that it is a vector that modulates not only the amplitude but also the direction of the inner winding flux. The outer air gap flux linkage equation in dq axis can be written as

$$\begin{bmatrix}\psi_{d1}\\ \psi_{q1}\end{bmatrix}=\begin{bmatrix}L_{d1}i_{d1}\\ L_{q1}i_{q1}\end{bmatrix}+\bar{\lambda}\begin{bmatrix}L_{d2}i_{d2}\\ L_{q2}i_{q2}\end{bmatrix} \tag{4}$$

in which ψ_{d1} and ψ_{q1} are respectively the d-axis and q-axis flux linkage of the outer stator, L_{d1},L_{q1} and L_{d2},L_{q2} are outer and inner winding inductances of d-axis and q-axis, and i_{d1},i_{q1} and i_{d2},i_{q2} are outer and inner winding currents of d-axis and q-axis.

According to the speed relations in Eq. (3) and the flux equation above, the voltage equation of the DFFM motor can be written as

$$\begin{aligned}\begin{bmatrix}u_{d1}\\ u_{q1}\end{bmatrix}&=\begin{bmatrix}R_1 i_{d1}\\ R_1 i_{q1}\end{bmatrix}+p\begin{bmatrix}L_{d1}i_{d1}\\ L_{q1}i_{q1}\end{bmatrix}\\&+\begin{bmatrix}-(\omega_r-\omega_2)L_{q1}i_{q1}\\ (\omega_r-\omega_2)L_{d1}i_{d1}\end{bmatrix}+\bar{\lambda}\begin{bmatrix}(\omega_r-\omega_2)L_{q2}i_{q2}\\ (\omega_r-\omega_2)L_{d2}i_{d2}\end{bmatrix}\end{aligned} \tag{5}$$

in which p is the differential operator, R_1 is the outer winding resistance, ω_r is the rotor rotating angular velocity, and the ω_2 is the magnetic field rotating velocity generated by the inner winding.

From (3)~(5), the torque equation of the DFFM motor is obtained as

$$\begin{aligned}T&=\frac{3}{2}\begin{bmatrix}-p_1\psi_{q1} & p_1\psi_{d1}\end{bmatrix}\begin{bmatrix}i_{d1}\\ i_{q1}\end{bmatrix}\\&=\frac{3}{2}p_1\left[\lambda_{d2}L_{d2}i_{d2}i_{q1}+(L_{d1}-L_{q1})i_{d1}i_{q1}\right]\end{aligned} \tag{6}$$

It can be derived from (6) that when $i_{d1}=0$, $i_{q2}=0$ strategy is proposed on the DFFM motor, the torque equation can be simplified as

$$T=\frac{3}{2}p_1\lambda_{d2}L_{d2}i_{d2}i_{q1} \tag{7}$$

As the outer stator pole pair number p_1, the modulation ratio λ_{d2} and the inner winding inductance L_{d2} are constant when motor manufacture is finished. Eq. (7) indicates that the torque of the proposed motor is is proportional to the outer winding q-axis current and the inner winding d-axis current as the inner winding is defined as field winding in this paper,. The d-axis current of the inner stator has the same contribution as the outer winding q-axis current.

B. The rotor flux estimation and sensorless control

According to the analysis of the Part A in the Section, the modulation ratio $\bar{\lambda}$ is key parameter for the torque performance and the control of the DFFM. This parameter is mainly defined by the stator winding design, and obviously will be affected by the manufacture. For the reason above, the outer air gap flux linkage cannot be both accurately and directly gained. In this paper, the outer air gap flux estimation algorithm is provided in which the outer stator voltage and current is needed for the estimation. The derivation of the algorithm is as below.

According to Eq.(4), the flux linkage equation of the outer stator winding of the DFFM in $\alpha\beta$ coordination system is gained as

$$\begin{aligned}&\begin{bmatrix}\cos\theta & -\sin\theta\\ \sin\theta & \cos\theta\end{bmatrix}\begin{bmatrix}\psi_{d1}\\ \psi_{q1}\end{bmatrix}\\&=\begin{bmatrix}\cos\theta & -\sin\theta\\ \sin\theta & \cos\theta\end{bmatrix}\begin{bmatrix}L_{d1} & 0\\ 0 & L_{q1}\end{bmatrix}\begin{bmatrix}\cos\theta & \sin\theta\\ -\sin\theta & \cos\theta\end{bmatrix}\begin{bmatrix}i_{\alpha1}\\ i_{\beta1}\end{bmatrix}\\&+\bar{\lambda}\begin{bmatrix}\cos\theta & -\sin\theta\\ \sin\theta & \cos\theta\end{bmatrix}\begin{bmatrix}L_{d2} & 0\\ 0 & L_{q2}\end{bmatrix}\begin{bmatrix}i_{d2}\\ i_{q2}\end{bmatrix}\end{aligned} \tag{8}$$

in which θ is the rotor position. When the control strategy of $i_{q2}=0$ is proposed on the DFFM motor, the above equation can be simplified as

$$\begin{aligned}\begin{bmatrix}\psi_{\alpha1}\\ \psi_{\beta1}\end{bmatrix}&=\begin{bmatrix}L_{d1}\cos^2\theta+L_{q1}\sin^2\theta & (L_{d1}-L_{q1})\cos\theta\sin\theta\\ (L_{d1}-L_{q1})\cos\theta\sin\theta & L_{d1}\cos^2\theta+L_{q1}\sin^2\theta\end{bmatrix}\begin{bmatrix}i_{\alpha1}\\ i_{\beta1}\end{bmatrix}\\&+\lambda_{d2}L_{d2}i_{d2}\begin{bmatrix}\cos\theta\\ \sin\theta\end{bmatrix}\end{aligned} \tag{9}$$

In Eq. (9), the rotor position information can be directly observed for the item $\lambda_{d2}L_{d2}i_{d2}\begin{bmatrix}\cos\theta\\ \sin\theta\end{bmatrix}$ from which θ can be gotten with an ATAN calculation.

The flux linkage of the outer winding can be calculated by measuring its voltage and the current, the relationship of them can be described as

$$\begin{bmatrix}\psi_{\alpha1}\\ \psi_{\beta1}\end{bmatrix}=\begin{bmatrix}\int(v_{\alpha1}-R_1\cdot i_{\alpha1})dt\\ \int(v_{\beta1}-R_1\cdot i_{\beta1})dt\end{bmatrix} \tag{10}$$

The position of the rotor can be estimated according to above equations (9) and (10). For clear explanation, the iterative procedure from (9) and (10) is described in Fig. 3.

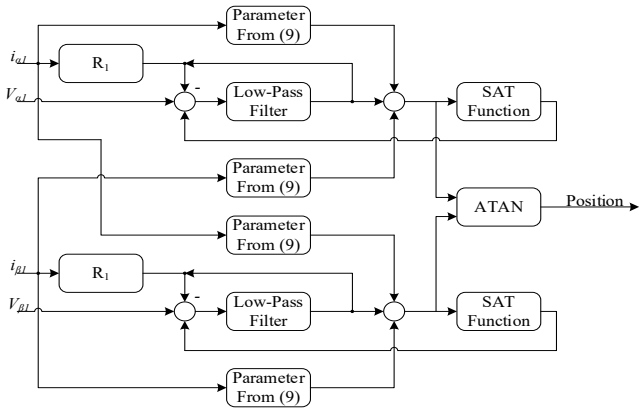

Fig. 3. Iterative rotor position estimation diagram of DFFM motor.

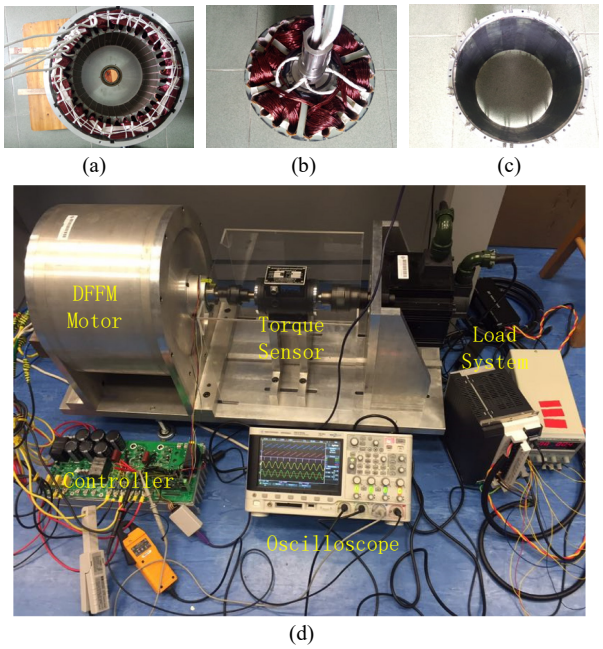

(a) (b) (c) (d)

Fig. 4 Motor design and experiment setup. (a) outer stator, (b) inner stator, (c) rotor, (d) experiment setup.

In the iterative procedure, the previous step rotor position is used for calculate the parameter matrix of i_α and i_β in Eq. (9), and the ψ_1 in $\alpha\beta$ axis can be calculated in Eq. (10). A saturation function here is used to avoid flux saturation, which can be represented as

$$f_{sat}(n)=\begin{cases} k & n<-mi_{d2} \\ -k & n>mi_{d2} \\ 0 & otherwise \end{cases} \tag{11}$$

in which k and m is gain of this estimation procedure. i_{d2} is included in the saturation function as it produces the rotor flux.

IV. Simulation And Experimental Results

A. Motor design and Experiment setup

The motor design and the experiment setup is as shown in Fig. 4. The motor parameters have been proposed in Table I, the outer diameter of the inner stator is 106mm, the thickness of the rotor is 8mm, the inner diameter of the outer stator is 121mm and both air gaps are 1mm. A resolver is connected to verify the real rotor position. The setup of the experiment is as shown in Fig. 4(d), a Panasonic Servo system is used as load of the DFFM motor and connects to the motor with a torque sensor. As the DFFM motor has two windings, a controller which has two sets of PWM outputs is used to drive the system, a digital to analog (DA) module is included so that measured and estimated motor position can be output as analog signals. An oscilloscope is used to measure the signals of currents and position.

B. Back-EMF result

The back-EMF experiment is used to verify the motor design. The inner winding has been supplied by 15A DC current, the motor is driven by the servo system and the outer winding phase voltages are measured, as has been described in section II, Fig. 2(a) to (e). The experiment result is as shown in Fig. 5, the time of the scope is 100ms/div.

It can be seen from the figure that when DFFM motor driven by the servo system at the speed of 900RPM and 15A DC current supplied in the inner winding, the magnetic flux can be produced in the outer air gap, which induces the sinusoid voltage in the out windings.

C. Sensorless control Simulation result

In this part, the sensorless control simulation result is proposed as shown in Fig. 6. An eight seconds Matlab Simulink is used to verify the DFFM motor and its control strategy, the simulation setup is as below:

The load of the motor is constant as 1Nm and the target speed is 40rad/s. The main winding and auxiliary winding have the same resistance as 2.8 Ohm and the same inductance as 10 mH. The modulation ratio λ_{d2} is defined as 0.25.

From start of the simulation to the time of 2 seconds, the auxiliary winding is supplied a 0.5A DC current to help with the position estimation startup, during this time, the main winding current is 50A and its electrical speed is 40rad/s. At 2 seconds, the auxiliary winding electrical speed changes to 10 rad/s, and the main winding speed reduces to 30rad/s accordingly. At 4 seconds, the auxiliary winding current changes from 0.5A to 1A, thus the main winding current reduces to 25A as load does not change. At 6 seconds, the phase angle of the auxiliary changes suddenly, the main winding current phase changes accordingly.

It can be seen from Fig. 6 that during the whole simulation period, the estimation position is very close to the real position and the estimation error is very small.

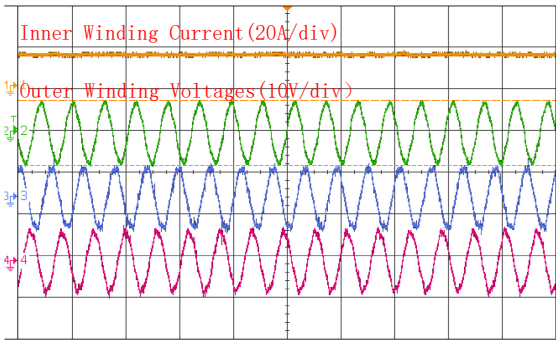

Fig. 5. Outer winding back-EMF when 15A DC current proposed in the inner winding at 900RPM.

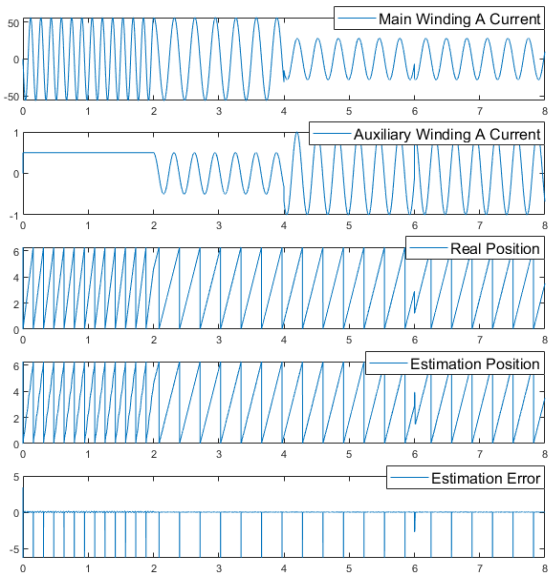

Fig. 6. DFFM motor sensorless control Simulation Result.

D. *Sensorless control experimental result*

According to Eq.(5)~(11), the DFFM motor can be controlled. In this part, a constant torque load is generated by the Panasonic servo system and the control result of the DFFM motor is shown and analyzed in different stages.

In Fig. 7~10, the real and estimated outer air gap magnetic flux angle and the corresponding error are measured by the oscilloscope. The real angle is measured by DFFM controller using the resolver connected to the motor. Both the real and estimated position is output by the controller with the DA module. The error is calculated by the oscilloscope itself. The outer and inner winding phase currents (both Phase C here) are also measured.

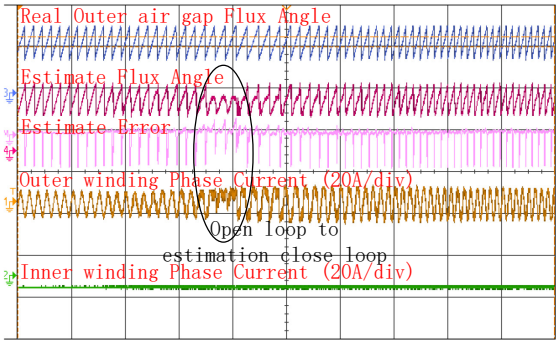

Fig. 7. Startup of the DFFM control

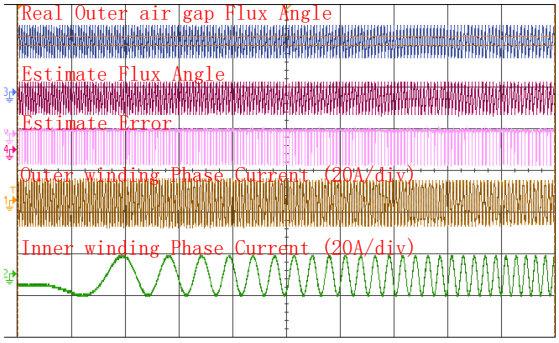

Fig. 8. Control result when inner winding current changes from DC to AC

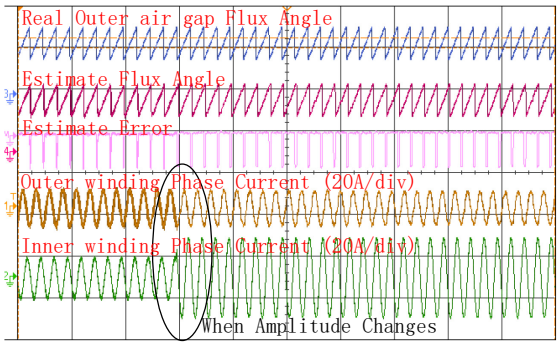

Fig. 9. Sensorless control result when amplitude of the inner winding current changes.

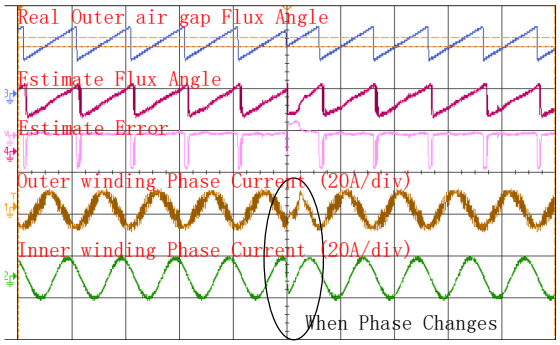

Fig. 10. Sensorless control result when phase angle of the inner winding current changes

1) *Sensorless startup with DC excitation in inner winding*

The startup experiment is to show how position estimation procedure starts. The startup of the sensorless procedure is open loop and then changes to position close loop. For inner winding set, $i_{q2}=0$ and $\omega_2=0$ strategy is proposed, which generates DC current to the inner winding. The equation (5) and (6) will be very similar as a permanent magnet synchronous motor (PMSM), the only different is that the inner winding generated magnetic field in DFFM motor is instead of the rotor PM magnetic field in PMSM. Thus the startup to the DFFM motor is similar to the PMSM sensorless startup.

At the beginning of the open loop startup, for the outer winding, a $i_{q1}=0$ and $\omega_1=0$ strategy is also proposed. The rotor is aligned to the beginning position and estimation algorithm starts to work. After alignment, the constant voltage frequency ratio strategy is proposed in the outer winding and the rotor speed increases gradually, during this stage, the estimation algorithm continues calculate to estimate the rotor position. When estimate position and open loop position is close enough, the system changes to the estimation close loop stage. In this stage, the estimation position is used in the control system and rotating speed goes to the rated speed. The changes from open loop to the estimation close loop is as shown in the Fig. 7, the time of the scope is 500ms/div.

In Fig. 7, the changes from open loop to the estimation close loop is marked strikingly. The inner winding phase current keeps constant as DC current is supplied in this stage. Before the change, the rotor speed is slow, the estimation error is small enough so that the control strategy starts changing, after 3 to 4 electrical cycles (which is about a quarter of real rotating circle),

the strategy changes successfully from open loop to close loop. The outer winding current is slightly bigger because the motor starts to accelerate.

In particular, in Fig. 7, Phase C current is measured and it's not the max value when a DC current supplied to a 3-phase system.

2) Sensorless control when AC excitation in inner winding

The DC to AC excitation change is similar as shown in Part C at the time of 2 seconds. After startup, the inner winding current can be changes from DC to AC, which means ω_2 accelerate from 0 speed, the rotor speed keeps constant during the whole changes. According to Eq. (3), $f_1 + f_2$ is a constant if rotor speed keeps constant. Then change from DC excitation to AC excitation is as shown in Fig. 8, the time of the scope is 500ms/div.

It can be seen from Fig. 8 that inner winding phase current changes from DC to AC and its frequency accelerates gradually. With inner winding frequency increases, the outer winding frequency decreases correspondingly, the sum of them keeps constant as rotor speed keeps constant. The out air gap flux frequency decreases due to the current frequency decreases and the estimation algorithm still works steadily.

In particular, in Fig. 8, the amplitude of the inner winding current keeps constant whether it is DC current or AC current, only frequency changes.

The above two experiment verifies the DFFM sensorless control algorithm, the frequency of the two windings can change freely. To reduce the switching losses of the control unit, the working frequencies of the two winding are set to be equal.

3) When amplitude of the i_2 changes

The amplitude of i_2 change is similar as shown in Part C at the time of 4 seconds. According to Eq. (7), the amplitude of the inner and outer winding currents is related to the torque performance. It is easy to known from the equation that keeps the equal amplitude of the two winding sets is the most efficient control strategy. As inner and outer winding current should keep equal, the amplitudes of them may change when load torque changes. The performance of the position estimation algorithm in this situation should be evaluated.

In this experiment, the sensorless performance when inner winding amplitude changes is evaluated. The load torque keeps constant, and inner winding current's amplitude step changes to see whether estimation algorithm can work. As current changing speed is much faster than torque changing speed, this experiment's situation is more strictly than toque changes. The result is as shown in Fig. 9, the time of the scope is 100ms/div.

In Fig. 9, the amplitude change has been marked strikingly. It can be seen from the figure that amplitude of inner winding current changes, the estimation procedure still works well. The outer winding current decreases correspondingly as the load torque does not change. This can be explained according to Eq. (11), the saturation of the estimation flux feedback is related to i_{d2}, this makes the outer flux estimation more accurate when inner winding current changes.

4) When phase of the i_2 changes

The phase of i_2 change is similar as shown in Part C at the time of 6 seconds.As the performance when amplitude change has been discussed in the above part, the performance when phase of the excitation changes can also be evaluated. The result is as shown in Fig. 10, the time of the scope is 20ms/div for clearly.

In Fig. 10, the phase change has been marked strikingly. The phase angle of the inner winding is controlled to change 180 degree, thus the phase of sinusoid current has a step change, after transient instability, the estimation flux angle has reaches to the real angle again, which leads the outer winding current also changes its phase. After milliseconds, the system continue works again. This can be explained with Eq. (9), the controlled changes of the angle value can be set in the old angle value, this can help the estimation comes to steady again more quickly.

The above two experiments verify the steady performance of the designed estimation algorithm, the results show that it can work when inner winding current has amplitude or phase changes.

V. Conclusion

A new flux estimation based sensorless control method for a DFFM motor is proposed in this paper. As the DFFM has two stator windings and one rotor, either the inner stator winding or the outer stator winding can be the field winding, and then the other stator winding can be controlled for torque generation. Therefore, the sensorless control strategy should consider the control of both the two sets of windings. Furthermore, the phase and amplitude of the excitation current are all considered in the proposed improved flux estimation observer. When the frequency, the amplitude or phase angle of the field winding changes during the operation, the sensorless control is still doing well and the estimated error is small as shown simulation and experimental results. It means the proposed sensorless control method based on Eq. (9) and (10) fits well for the speed and torque control of DFFM.

References

[1] Li, D., R. Qu and J. Li, "Topologies and analysis of flux-modulation machines," *IEEE Energy Conversion Congress and Exposition (ECCE)*, 2015.

[2] Rens, J., et al., "Design, analysis and realization of a novel magnetic harmonic gear," *18th International Conference on Electrical Machines*. 2008.

[3] Wang, L.L., et al., "A novel magnetic-geared outer-rotor permanent-magnet brushless motor," *4th IET Conference on Power Electronics, Machines and Drives*, Stevenage, 2008.

[4] Liu, Z., et al., "Electromagnetic performance of double-stator flux-modulation permanent-magnet motor," *IEEE Transactions on Applied Superconductivity*, vol. 26, no. 4, p. 1-5, 2016.

[5] Zhou, H., et al., "A novel five-phase double-stator tubular fault-tolerant flux-modulation permanent magnet motor," *IEEE Transactions on Applied Superconductivity*, vol. 28, no. 3, pp. 1-5, 2018.

[6] Sheng, T., et al., "Topology exploration and torque component analysis of double stator biased flux machines based on magnetic field modulation mechanism," *IEEE Transactions on Energy Conversion*, vol. 33, no. 2, p. 584-593, 2018.

[7] Cheng, M., P. Han and W. Hua, "General airgap field modulation theory for electrical machines," *IEEE Transactions on Industrial Electronics*, vol. 64, no. 8, p. 6063-6074, 2017.

[8] Wang, Y., S. Niu and W. Fu, "A novel dual-rotor bidirectional flux-modulation PM generator for stand-alone DC power supply," *IEEE*

Transactions on Industrial Electronics, vol. 66, no. 1, p. 818-828, 2019.

[9] Chau, K.T., et al., "Design of a magnetic-geared outer-rotor permanent-magnet brushless motor for electric vehicles," *IEEE Transactions on Magnetics*, vol. 43, no. 6, p. 2504-2506, 2007.

[10] Jang, D. and J. Chang, "Effects of flux modulation poles on the radial magnetic forces in surface-mounted permanent-magnet vernier machines," *IEEE Transactions on Magnetics*, vol. 53, no. 6, p. 1-4, 2017.

[11] Niu, S., et al., "Quantitative comparison of novel vernier permanent magnet machines," *IEEE Transactions on Magnetics*, vol. 46, no. 6, p. 2032-2035, 2010.

[12] Wang, L.L., et al., "Development of a Magnetic-Geared Permanent-Magnet Brushless Motor," *IEEE Transactions on Magnetics*, vol.45, no. 10, p. 4578-4581, 2009.

[13] Zou, T., et al., "Performance Comparison of Surface and Spoke-Type Flux-Modulation Machines With Different Pole Ratios," *IEEE Transactions on Magnetics*, vol. 53, no. 6, p. 1-5, 2017.

[14] Luo, X. and S. Niu, "A novel contra-rotating power split transmission system for wind power generation and ilts dual MPPT control strategy," *IEEE Transactions on Power Electronics*, vol. 32, no. 9, p. 6924-6935, 2017.

[15] Smith, A.N., S.M. Gadoue and J.W. Finch, "Improved rotor flux estimation at low speeds for torque MRAS-based sensorless induction motor drives," *IEEE Transactions on Energy Conversion*, vol. 31, no. 1, p. 270-282, 2016.

[16] Stojic, D., et al., "Improved stator flux estimator for speed sensorless induction motor drives," *IEEE Transactions on Power Electronics*, vol. 30, no. 4, p. 2363-2371, 2015.

[17] Zhao, R., et al., "A novel flux estimator based on multiple second-order generalized integrators and frequency-locked loop for induction motor drives," *IEEE Transactions on Power Electronics*, vol. 32, no. 8, p. 6286-6296, 2017.

Xiang Luo received the B.Sc., M.Sc., and Ph.D. degrees in electrical engineering from the School of Electrical Information and Electrical Engineering, Shanghai Jiao Tong University, Shanghai, China, in 2005, 2009, and 2013, respectively. Since 2013, he has been with the Shanghai Jiao Tong University, where he is currently a Research Associate in the School of Electrical Information and Electrical Engineering. His research interests include electrical machines, motor drives for electric vehicles, renewable energy generation, and applied electromagnetics.

L. Zhu received the B.Sc. in Electrical Engineering and Automation from the Shanghai Jiao Tong University (SJTU), Shanghai, China in 2003, and received the B.Sc. and Ph.D. degree in Electric Machines and Apparatus from SJTU respectively in 2006 and 2009. After receiving the PhD degree, she was a PostDoc and associate researcher of Wisconsin Electric Machines and Power Electronics Consortium (WEMPEC) in University of Wisconsin-Madison, working on the design and optimization of direct-drive wind power generator. Since December 2011, she is the associate professor of Electric Machines and Apparatus, SJTU. Her research interest includes machine analysis and optimization, and design and control of special machine

Xu Cai received the B.Eng. degree in electrical engineering from Southeast University, Nanjing, China, in 1983. He received the M.Sc. and Ph.D. degrees from China University of Mining and Technology, Beijing, China, in 1988 and 2000, respectively. He was with the Department of Electrical Engineering, China University of Mining and Technology, as an Associate Professor from 1989 to 2001. He joined Shanghai Jiao Tong University, as a Professor from 2002 and has been the Director of Wind Power Research Center, Shanghai Jiao Tong University since 2008. His special fields of interest lie in power electronics and renewable energy exploitation and utilization.

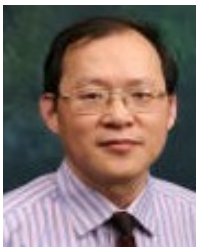

W. N. Fu received the B.Eng. degree in electrical engineering from Hefei University of Technology, Hefei, China, in 1982, the M.Eng. degree in electrical engineering from Shanghai University of Technology, Shanghai, China, in 1989, and the Ph.D. degree in electrical engineering from Hong Kong Polytechnic University, Hong Kong, in1999. He is currently a Professor at Hong Kong Polytechnic University. Before joining the university in October 2007, he was one of the Key Developers at Ansoft Corporation, Pittsburgh, PA, USA. He has about seven years of working experience at Ansoft, focusing on the development of the commercial software Maxwell. He has published 184 papers in refereed journals. His current research interests mainly include numerical methods of electromagnetic field computation, optimal design of electric devices based on numerical models, applied electromagnetics, and novel electric machines.

Xinye Wu received the B.Eng. degree Shanghai University of Engineering, Science, Shanghai, China, in 2001. He joined State Grid Shanghai Municipal Electric Power Company, Shanghai, China, in 2001, and was engaged in the overhaul of primary equipment, electrical test and on-site detection of substation. Since 2010, he has worked in the management department of State Grid Shanghai Municipal Electric Power Company, Shanghai, China. His work focuses on the technical management of live detection of transformer equipment and primary transformer equipment.